

Using the Quantum Zeno Effect for Suppression of Decoherence

Yasushi Kondo

Department of Physics, Kinki University, Higashi-Osaka 577-8502, Japan

E-mail: ykondo@kindai.ac.jp

Yuichiro Matsuzaki

NTT Basic Research Laboratories, NTT Corporation, Kanagawa 243-0198, Japan

Kei Matsushima

Department of Physics, Kinki University, Higashi-Osaka 577-8502, Japan

Jefferson G. Filgueiras

Fakultät Physik, Technische Universität Dortmund, Otto-Hahn-Strasse 4, D-44221 Dortmund, Germany

Instituto de Física de São Carlos, Universidade de São Paulo, P.O. Box 369, São Carlos, 13560-970 SP, Brazil

August 2015

Abstract. Projective measurements are an essential element of quantum mechanics. In most cases, they cause an irreversible change of the quantum system on which they act. However, measurements can also be used to stabilize quantum states from decay processes, which is known as the Quantum Zeno Effect (QZE). Here, we demonstrate this effect for the case of a superposition state of a nuclear spin qubit, using an ancilla to perform the measurement. As a result, the quantum state of the qubit is protected against dephasing without relying on an ensemble nature of NMR experiments. We also propose a scheme to protect an arbitrary state by using QZE.

PACS numbers: 03.67.Pp, 03.65.Xp, 76.60.-k

Keywords: Quantum Zeno Effect, Decoherence Suppression, NMR

Submitted to: *New J. Phys.*

1. Introduction

Interactions between a quantum system and its environment lead to changes of the system state and can result in the loss of coherence. This effect, often called decoherence, is a limiting factor for many applications, such as quantum computing. The loss of information associated with this process can be measured by the decreasing overlap between the initial and current states. This overlap (state fidelity) changes quadratically for times short enough compared to the inverse of the strength of the system-environment coupling and the correlation time of the environment, provided this coupling is also static on the relevant timescale [1, 2]. If such a system is repeatedly projected back to the original state by measurements performed before the state has changed significantly, the effect of the system-environment interaction can be effectively eliminated in the limit of sufficiently frequent measurements. This is termed the Quantum Zeno Effect (QZE) [3]. There are many potential applications of QZE, like entanglement generation [4], quantum metrology [5, 6], and quantum imaging [7].

It is worth mentioning that QZE is different from dynamical decoupling, which also suppresses decoherence. Although both schemes were unified from the viewpoint of a strong interaction between a system of interest and the others [8], there is a clear difference between them. While dynamical decoupling uses unitary control to average out the system-environment interaction [9], the non-unitary dynamics introduced by the measurements is essential for the state stabilization in QZE.

In the simplest case, the evolution suppressed by QZE is driven by a single interaction to a static external degree of freedom. Typical examples include a transition between two states of a single trapped ion [10], nuclear magnetic resonance (NMR) [11], and atomic systems [12, 13]. Another example is the confinement of a unitary dynamics in a specific subspace, as demonstrated in a rubidium Bose Einstein condensate [14]. In a more sophisticated case, QZE restrains the non-unitary dynamics of an open quantum system [3], instead of suppressing a unitary evolution driven by external fields. One experiment controlled such non-unitary dynamics, the escape rate of atoms from a trap, using the QZE [15]. However, QZE to suppress the dephasing of a two-level system was not demonstrated yet.

In this paper, we present a proof-of-principle demonstration that QZE is equally possible to stabilize the state of a quantum system subject to dephasing by successive measurements. We employ a liquid-state NMR Quantum Computer with a two-spin molecule. However, the ensemble nature of NMR is not essential to implement the measurements in our experiments, unlike in [11, 16]. A similar scheme was proposed for a non-ensemble system in [17]. Also, QZE experiments without relying on an ensemble average were reported [18].

This paper is organized as follows. In Sec. II, a brief review on QZE and a detailed theoretical background of our experiment are presented. We show a proof-of-principle demonstration, including a characterization of the molecule employed in our experiments, in Sec. III. The last section is devoted to conclusion and discussions,

where we propose a scheme to protect an arbitrary state by using QZE.

2. Theory

2.1. Quantum Zeno Effect

In order to understand the essence of QZE, it is sufficient to consider a coherent superposition of a qubit being dephased by a randomly fluctuating classical field [1, 2], with the concept of “mixing process” [19]. The relevant Hamiltonian is thus

$$\mathcal{H}(t) = H_s + H_I + H_{en}, \quad (1)$$

$$H_s = \frac{\omega_s}{2}\sigma_z, \quad (2)$$

$$H_I = \lambda\sigma_z\hat{A}, \quad (3)$$

$$H_{en} = \omega_{en}\hat{B}, \quad (4)$$

where ω_s denotes the energy of the system, λ denotes the strength of the fluctuating field, \hat{A} denotes the environmental operator to represent the interaction with the system, ω_{en} denotes the environmental energy, \hat{B} denotes the environmental operator, and σ_i is a Pauli matrix. The Hamiltonian contains only σ_z because only pure dephasing is considered. We go to an interaction picture, obtaining

$$H_I(t) \simeq \lambda\sigma_z\hat{A}(t), \quad (5)$$

where $\hat{A}(t) = e^{i\omega_{en}\hat{B}}\hat{A}e^{-i\omega_{en}\hat{B}}$.

We prepare a superposition state $|+\rangle = \frac{1}{\sqrt{2}}(|0\rangle + |1\rangle)$ for the system. The density matrix of the system and the environment is $\rho(0) = \rho_s(0) \otimes \rho_{en}$ where $\rho_s(0) = |+\rangle\langle+|$ and ρ_{en} denotes the initial state of the environment. Formally integrating the von Neumann equation $\dot{\rho} = -i[\mathcal{H}, \rho]$, we obtain

$$\rho(t) = \rho(0) - i\lambda \int_0^t dt_1 [\sigma_z\hat{A}(t_1), \rho(t_1)].$$

The natural unit system with $\hbar = 1$ is used. Iterating $\rho(t_1)$ on the right hand side and replacing $\rho(t_2)$ by $\rho(0)$, we have the second order expression

$$\begin{aligned} \rho(t) \simeq & \rho(0) - i\lambda \int_0^t dt_1 [\sigma_z\hat{A}(t_1), \rho(0)] \\ & - \lambda^2 \int_0^t \int_0^{t_1} dt_1 dt_2 [\sigma_z\hat{A}(t_1), [\sigma_z\hat{A}(t_2), \rho(0)]]. \end{aligned}$$

Tracing out the environment, we get

$$\rho_s(t) = \rho_s(0) - \lambda^2 \int_0^t \int_0^{t_1} dt_1 dt_2 \langle \hat{A}(t_1)\hat{A}(t_2) \rangle [\sigma_z, [\sigma_z, \rho_s(0)]]. \quad (6)$$

where $\rho_s(t) = \text{Tr}_{en}[\rho(t)]$ denotes the density operator of the system, $\text{Tr}_{en}[\dots]$ denotes a partial trace of the environment, and $\langle \hat{A}(t_1)\hat{A}(t_2) \rangle = \text{Tr}[\hat{A}(t_1)\hat{A}(t_2)\rho_{en}]$ denotes a correlation function. Here, we assume an unbiased noise $\langle \hat{A}(t) \rangle = \text{Tr}[\hat{A}(t)\rho_{en}] \simeq 0$ and a time symmetry $\langle \hat{A}(t_1)\hat{A}(t_2) \rangle = \langle \hat{A}(t_2)\hat{A}(t_1) \rangle$.

If the correlation time of the noise is much shorter than the relevant time scale of the system [20], the duration of each measurement in our case, we can approximate the correlation function by a δ -function

$$\langle \hat{A}(t_1)\hat{A}(t_2) \rangle = 2\tau_c\delta(t_1 - t_2),$$

where τ_c is the correlation time. Substituting into Eq. (6), we have $\rho_s(t) \simeq \rho_s(0) - \lambda^2\tau_c t[\sigma_z, [\sigma_z, \rho_s(0)]]$. The state fidelity $F(t) = \langle +|\rho_s(t)|+ \rangle$ is then

$$F(t) \simeq 1 - 2\lambda^2\tau_c t, \quad (7)$$

which corresponds to a linear decay. It is a well known fact QZE is not observable in this regime [3].

In the opposite limit of a slowly fluctuating environment, where $|t_1 - t_2| \ll \tau_c$, the correlation function is constant,

$$\langle \hat{A}(t_1)\hat{A}(t_2) \rangle = 1,$$

and Eq. (6) becomes $\rho_s(t) \simeq \rho_s(0) - \frac{1}{2}\lambda^2 t^2[\sigma_z, [\sigma_z, \rho_s(0)]]$ for $\lambda^2\tau_c t \ll 1$, i.e., the decoherence quadratically starts:

$$F(t) \simeq 1 - \lambda^2 t^2. \quad (8)$$

This is the regime the QZE can be observed: if N sequential projective measurements of $|+\rangle\langle+|$ are carried out on the system and the delay between the measurements is short compared to the correlation time, $T/N \ll \tau_c$, the system remains in the initial state with a probability $P(N) = (F(T/N))^N \simeq \left(1 - \frac{\lambda^2 T^2}{N^2}\right)^N \simeq e^{-\frac{\lambda^2 T^2}{N}}$. Since the exponent can become arbitrarily small for large N , the decoherence vanishes asymptotically.

2.2. Theoretical Background of Experiment

We intend to show a proof-of-principle demonstration with NMR that QZE is employed for protecting a phase decoherence. We need to answer two questions: 1) how to obtain a system that shows a quadratic decay. 2) how to measure a quantum system without employing ensemble averages, unlike usual NMR experiments [11, 16].

2.2.1. Quadratic Decay. A molecule in a solvent strongly and rapidly interacts with molecules of the solvent. These interactions are so strong and rapid that they effectively cancel with each other. Therefore, the effective interaction between the molecule and the solvent is often small [21]. This phenomenon is called motional narrowing. Since T_1 and T_2 of a spin in the molecule become longer, peaks in its NMR spectrum become sharper. The total number of quantum gates that can be performed within the coherence time is estimated as T_2/τ_G , where τ_G denotes the time of the gate operation. These long T_2 guarantees many quantum operations and liquid state NMR is often employed to demonstrate quantum algorithms.

We introduce molecules with magnetic dipole moments, originated from electrons, into the solvent. These molecules generate strong but short range magnetic fields. They

are short range in the sense that they decay with r^{-3} or faster as a function of r , the distance. These molecules are called magnetic impurities. They also move rapidly in the solvent. When a magnetic impurity passes by a molecule, a strong interaction between a spin in the molecule and the magnetic impurity changes the spin state abruptly. Such an interaction leads to a final spin state uncorrelated to the initial one. Motional narrowing does not occur, since there are not enough magnetic impurities for their effects to be canceled on average.

The interaction of the spin with the magnetic impurity is a δ function-like in time, and thus we do not expect a quadratic decay of the spin state. The higher density of the magnetic impurity leads to shorter T_1 and T_2 , but the characteristic of the state decay is always linear, like in Eq. (7).

Now, let us consider a two-spin molecule. One of the two spins (called E) is under the influence of a magnetic impurity and interacts with the other spin (called S) through a scalar coupling (for simplicity, the weak coupling limit [22] is assumed)

$$\mathcal{H}_J = J\sigma_z^S\sigma_z^E/4, \quad (9)$$

where σ_i^E (σ_i^S) is a Pauli operator acting on the spin E (S). J is the strength of the scalar coupling, in frequency units. The spin S interacts only with the spin E and free from the magnetic impurity. The delta function-like interaction on the spin E due to the magnetic impurity is transformed into a slower interaction on the spin S by the scalar coupling. In this case, J and T_1 of the spin E determine the correlation time. However, for the case considered in this paper, the J term is more essential in the practical range of T_1 of the spin E and the correlation time becomes of the order of $2\pi/J$.

We can obtain a spin showing a quadratic decay with a two-spin molecule and magnetic impurities. The correlation time is of the order of $2\pi/J$, usually of few milliseconds for a carbon and hydrogen nuclei combination and thus this interaction is well controllable with NMR techniques. A similar approach has been reported, but using a series of pulses instead of magnetic impurities [19].

2.2.2. Projective Measurements. A field gradient was often employed as a projective measurement in NMR experiments [11, 16]. However, it is based on a spacial averaging, or the ensemble nature of NMR, and thus it is considered as a mere simulation of a projective measurement. Therefore, we cannot employ a field gradient as a projective measurement in our experiment.

We have to implement a measurement according to its definition. A measurement of a system means the system is entangled to a measurement apparatus. Then, the measurement apparatus falls into one of its eigenstates. The corresponding eigenvalue is treated as the measured value [23]. According to this idea, we are able to implement a non-selective measurement M_{DS} with another qubit, called a device (D), as follows

$$M_{DS}(\rho) = \frac{1}{2}Ad(\mathcal{E}_1, \rho) + \frac{1}{2}Ad(\mathcal{E}_2, \rho), \quad (10)$$

where $Ad(*, \rho) = *\rho*^\dagger$, $\mathcal{E}_1 = CNOT_{DS}$ and $\mathcal{E}_2 = \sigma_y^D CNOT_{DS}$. $CNOT_{DS}$ is a CNOT gate whose control and target qubits are the device D and the system S, respectively. We

employ $CNOT_{DS}$ as an entangler, while σ_y^D causes the phase decoherence of the device D [24]. This measurement operation is virtual and instantaneous. This procedure is effective when the system and device are not correlated before the measurements are performed. Such condition is satisfied, since the device is perfectly decohered by the operator σ_y^D at the end of each measurement.

It is worth mentioning that we use a stochastic master equation to describe the measurement, and such a master equation usually requires an average of the measurement outcomes [20]. However, the average technique is not against the fact that our scheme does not rely on the nature of ensemble average. Even for a single spin, one needs to repeat the experiment many times, and needs to take an average of the measurement results. For example, in [25], they consider a single NV center, and a model similar to ours is applied to include the fluctuating noise, using an average. Similarly, our calculation described here can be applied to a single spin.

2.2.3. QZE Simulation. We combine the ideas in § 2.2.1 and § 2.2.2 to design an ideal QZE simulation. We consider a three-qubit system. The first qubit is a system S of which phase is protected. The second qubit E mediates and filters the random noise caused by a magnetic impurity to the system. The third qubit is a device D.

First, we consider a time development without M_{DS} as follows.

$$[\tau_{xy}]^N, \quad (11)$$

where τ_{xy} is the period when the system decoheres and N is the number of repetitions. We describe the open system dynamics with the operator sum formalism [26]. The density matrix change during τ_{xy} is

$$\rho \rightarrow (1 - p_e \tau_{xy}) Ad(e^{-i\mathcal{H}_J \tau_{xy}}, \rho) + p_e \tau_{xy} Ad((\sigma_x^E \cos \theta + \sigma_y^E \sin \theta) e^{-i\mathcal{H}_J \tau_{xy}}, \rho), \quad (12)$$

where p_e determines the strength of decoherence, σ_i^E is a σ_i operator acting on the spin E, and θ is a random variable indicating the rotation axis of the π -rotation on the spin E, caused by the magnetic impurity. p_e is a function of the concentrations of the magnetic impurity and the molecule of interest. Since the initial state of E is $|0\rangle\langle 0|_E$ and H_J contains only σ_z^E , $Ad((\sigma_x^E \cos \theta + \sigma_y^E \sin \theta)^n, |0\rangle\langle 0|_E)$ is equivalent to $Ad((\sigma_y^E)^n, |0\rangle\langle 0|_E)$ for the interaction H_J , where n is an arbitrary integer. Therefore, we can replace the second term of $\sigma_x^E \cos \theta + \sigma_y^E \sin \theta$ by σ_y^E . We show the simulation results (red and green) with $p_e = 0.05$ and 0.00 in figure 1. The initial state is $|+\rangle\langle +|_S \otimes |0\rangle\langle 0|_E \otimes |0\rangle\langle 0|_D$. figure 2 shows the differences between simulations of $p_e = 0.05$ (red) and 0.00 (green) in the initial stage of the dynamics, shown in figure 1. A quadratic behaviour is observed.

Second, we introduce M_{DS} as follows.

$$[\tau_{xy} - M_{DS}]^N \quad (13)$$

We show the simulation results with $p_e = 0.05$ and three different τ_{xy} 's in figure 1. The result with $\tau_{xy} = 1/40$ (black) decays faster than that of $\tau_{xy} = 1/160$ (red), as expected. The result with $\tau_{xy} = 1/10$ decays even faster than the envelope of the simulated FID.

Figure 1. Simulated FID signal with $p_e = 0.05$ by Eq. (11) (large red) that shows oscillatory behaviour but decays in time. The data without decay (green) is the case of $p_e = 0$ and is shown for comparison. The three curves without oscillatory behaviours are simulations with the measurement M_{DS} . The red curve with $\tau_{xy} = 1/160$ decays slower than the black one, with $\tau_{xy} = 1/40$, as expected. The blue curve (dots) with $\tau_{xy} = 1/10$ decays even faster than the envelope of the simulated FID signal.

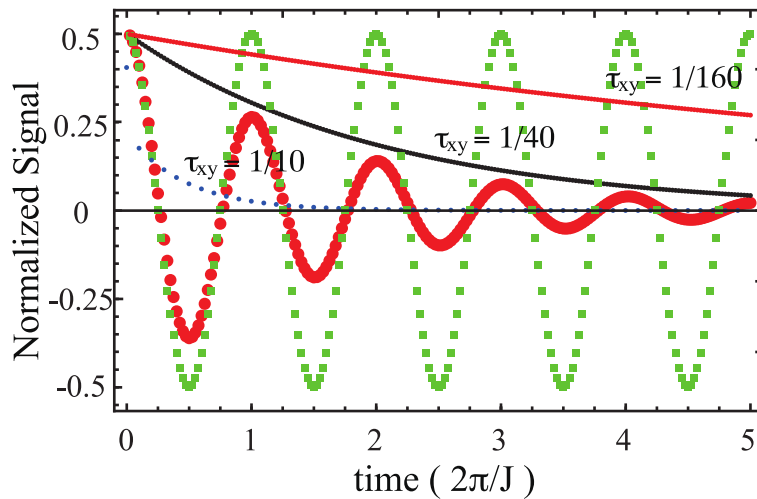
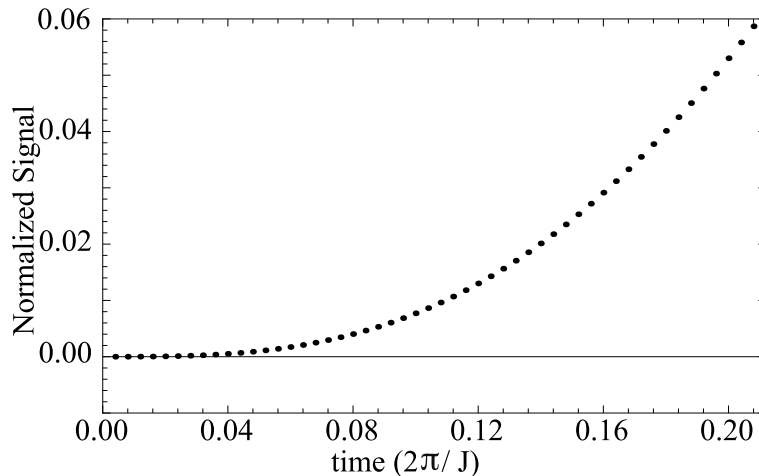


Figure 2. The differences between simulations with $p_e = 0.05$ (red) and 0.00 (green) in the initial stage of the dynamics, shown in figure 1. A quadratic behaviour is observed.



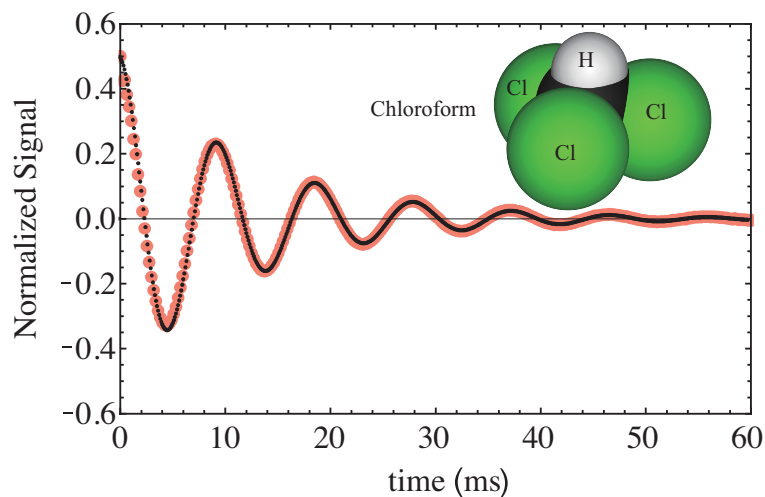
We can obtain the same results of figure 1 with M_{ES} , where E is the spin mediating the random noise. M_{ES} is obtained replacing $CNOT_{DS}$ and σ_y^D (equivalent with $\sigma_x^D \cos \theta + \sigma_y^D \sin \theta$) in Eq. (10) with $CNOT_{ES}$ and $\sigma_x^E \cos \theta + \sigma_y^E \sin \theta$ (equivalent with σ_y^E), respectively. It implies that we are able to measure the system S with the spin E, without introducing the device (third spin) D.

3. Experiments and Simulations

3.1. Sample

Our spectrometer is a JEOL ECA-500. The experiments were carried out using a ^{13}C -labeled chloroform (Cambridge Isotopes) diluted in d_6 -acetone with a 303 mM concentration, at room temperature. We added a magnetic impurity (47.7 mM of Iron(III) acetylacetonate, a relaxation agent to control T_1 and T_2 in NMR experiments) to the solution, which mainly introduces a random flip-flop motion of the ^1H spin, since the carbon atom is surrounded and protected by three chlorine and one ^1H atoms, as illustrated in the inset of figure 3. This is a realization of the configuration discussed in § 2.2.1.

Figure 3. Measured (large red) and simulated (small black) FID signals of ^{13}C . The ^{13}C atom is in the center of the schematic chloroform molecule, surrounded by the ^1H and the three chlorine atoms. The selected parameters are $(T_d, 1/p_s) = (6.5, 300)$ ms. $T/N_t = 0.1$ ms in Eq. (17) is taken for the computation.

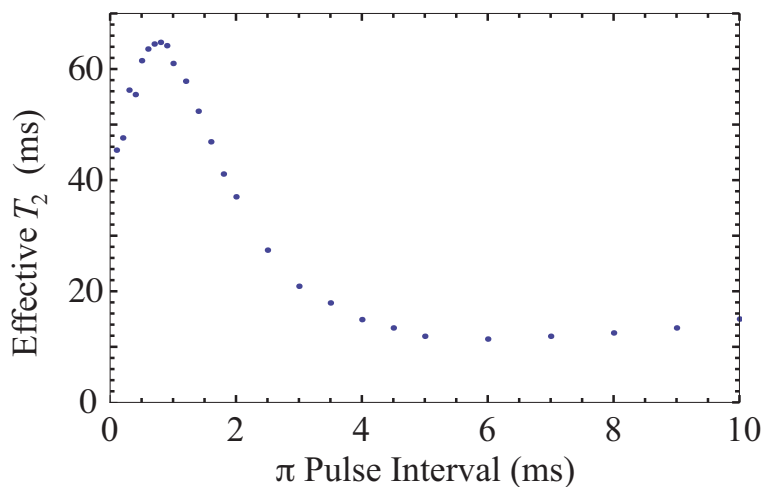


3.1.1. T_1 and T_2 Measurements and Bang-Bang Control To characterize the sample, we measured T_1 and T_2 of the ^1H and ^{13}C spins. T_1 and T_2 of the ^1H are both about 7 ms. It is reasonable because the magnetic impurity simultaneously flips spins and destroys their phase coherence. On the other hand, T_1 of the ^{13}C spin is 300 ms, while its T_2 is 17 ms. Without the magnetic impurities, T_1 and T_2 of the ^{13}C spin are 20 s and 0.3 s [27]. So, the T_2 relaxation is speed up by about 20 times. We measured T_1 using the standard inversion recovery sequence. Due to a good field homogeneity, T_2 can be obtained directly from the Free Induction Decay (FID) signal [22], see figure 3. This shorter T_2 , compared with T_1 , can be understood according to the discussion in § 2.2.1. For our sample, $J/2\pi \approx 215$ Hz.

We expect a quadratic decay in the FID signal as shown in figure 2. It is, however, difficult to observe such behaviour due to experimental limitations. Therefore, we

performed Bang-Bang controls on our sample, as shown in figure 4. Bang-Bang controls also require a quadratic decay to be effective and thus we are able to judge if our sample have it at the initial stage of decoherence. The effective T_2 of the ^{13}C is measured through the application of a XY-4 sequence [28, 29], which compensates pulse imperfections, to the ^{13}C spin. When the interval between the pulses is below 4 ms, the effective T_2 becomes longer. We observe a maximum in figure 4 which may be understood by the discussions in [30, 31]. We will consider this elsewhere.

Figure 4. Effective T_2 's of the ^{13}C spin as a function of the intervals between π -pulses of the XY-4 sequence applied to the ^{13}C spin.



Further, we also measured this effective T_2 applying a series of π -pulses to the ^1H spin, as shown in figure 5. If they are frequent enough, these π -pulses effectively decouple the ^1H and the ^{13}C spins, as well known in NMR [22]. The effective T_2 at the π -pulse interval of 0.2 ms becomes $97/17 \sim 6$ times longer than that without π -pulses. This result indicates that the dominant (more than 80 %) source of the decoherence of the ^{13}C spin is the ^1H one.

3.1.2. Simulation of the FID with operator sum formalism. We reproduce the observed FID signal shown in figure 3 using the operator sum formalism [26].

The thermal state density matrix of the two qubit system is well approximated as

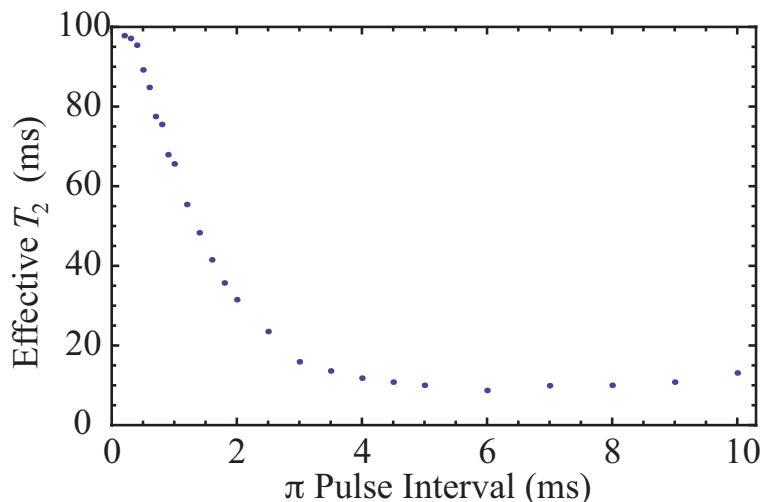
$$\rho = \left(\frac{\sigma_0}{2}\right)^{\otimes 2} + \epsilon_s \frac{\sigma_z \otimes \sigma_0}{4} + \epsilon_e \frac{\sigma_0 \otimes \sigma_z}{4}, \quad (14)$$

where $\epsilon_i = \hbar\omega_i/2k_B T$, ω_i is the Larmor frequency of the i -th spin, and σ_0 is the identity matrix of dimension 2. The suffixes s and e denote the ^{13}C and ^1H spin, respectively. Eq. (14) can be rewritten as

$$\rho = (1 - \epsilon_s) \left(\frac{\sigma_0}{2}\right)^{\otimes 2} + \epsilon_s |0\rangle\langle 0| \otimes \frac{\sigma_0}{2} + \epsilon_e \frac{\sigma_0 \otimes \sigma_z}{4}.$$

Since the trace of the NMR observable, such as $\sigma_{x,y}$, is zero, the term $(1 - \epsilon_s) (\sigma_0/2)^{\otimes 2}$ cannot be observed in NMR experiments and can be ignored. Moreover, only the ^{13}C

Figure 5. Effective T_2 's of the ^{13}C spin as a function of the intervals between π -pulses of the XY-4 sequence applied to the ^1H spin.



spin is observed (or, $\text{Tr}(\sigma_{x,y} \otimes \sigma_0, \rho)$ is measured), the above density matrix can be regarded as $\epsilon_s \rho_{\text{th}}$, where $\rho_{\text{th}} = |0\rangle\langle 0| \otimes (\sigma_0/2)$. This state can be normalized as a pseudopure state $|0\rangle\langle 0|$ for the ^{13}C spin, without any initialization operation.

The effect of the ^1H spin in the ^{13}C spin dynamics during the FID can be explained with Eq. (12) taking the ^1H spin as the spin E. p_e is given as $1/(2T_d)$ where T_d is the flip-flopping time constant. When the evolution time T is divided into N_t equal steps, the state after the i -th step is obtained as

$$\rho_{i+1} = \left(1 - p_e \frac{T}{N_t}\right) \text{Ad}(e^{-i\mathcal{H}_J T/N_t}, \rho_i) + p_e \frac{T}{N_t} \text{Ad}((\sigma_0 \otimes \sigma_y) e^{-i\mathcal{H}_J T/N_t}, \rho_i). \quad (15)$$

In our experiments, we also have to take into account a longitudinal relaxation of the ^{13}C spin, a process towards the thermal state, which is ρ_{th} in our case [24]. It can be described as

$$\rho_{i+1} = \left(1 - p_s \frac{T}{N_t}\right) \text{Ad}(e^{-i\mathcal{H}_J T/N_t}, \rho_i) + p_s \frac{T}{N_t} \rho_{\text{th}}, \quad (16)$$

where p_s is expected to be the inverse of T_1 of the ^{13}C spin.

When the dynamics of both the ^{13}C and ^1H spins are considered, the state after the i -th iteration is

$$\rho_{i+1} = \left(1 - (p_s + p_e) \frac{T}{N_t}\right) \text{Ad}(e^{-i\mathcal{H}_J T/N_t}, \rho_i) + p_e \frac{T}{N_t} \text{Ad}(\sigma_0 \otimes \sigma_y, \rho_i) + p_s \frac{T}{N_t} \rho_{\text{th}}, \quad (17)$$

where $(\sigma_0 \otimes \sigma_y) e^{-i\mathcal{H}_J T/N_t}$ is approximated as $\sigma_0 \otimes \sigma_y$. This approximation is valid because we take N_t such that $JT/N_t \ll 1$.

Black small dots in figure 3 show the simulated FID signal with $T/N_t = 0.1$ ms. Taking a proper parameter set of $(T_d, 1/p_s) = (6.5, 300)$ ms, our simulation reproduces the measured FID signal very well. T_d and $1/p_s$ are equal to $T_2(= T_1)$ of the ^1H spin and T_1 of the ^{13}C spin within experimental errors, respectively.

3.2. QZE Experiments

We take the ^{13}C and ^1H spins as S and E in § 2.2.3, respectively. We do not require a readout of the measurements, and thus a non-selective measurement is sufficient to observe the QZE. The initial state for our experiments is $|+\rangle\langle+| \otimes \sigma_0/2 = \text{Ad}(e^{-i\frac{\pi}{2}\sigma_y/2} \otimes \sigma_0, \rho_{\text{th}})$, obtained applying a $\pi/2$ pulse to the thermal state ρ_{th} .

3.2.1. Implementation of Non-Selective Measurements. The essential role of the *CNOTs* in M_{ES} and M_{DS} in § 2.2 is to entangle the two spins. So, we are able to employ another entangler, $e^{-i\pi\sigma_z \otimes \sigma_z/4}$ [32], which is locally equivalent to the *CNOT* employed in M_{ES} . Our measurement procedure is as follows,

- (i) applying $e^{\pm i\frac{\pi}{2}\sigma_y/2} \otimes \sigma_0$
- (ii) a time delay τ_z
- (iii) applying $e^{\mp i\frac{\pi}{2}\sigma_y/2} \otimes \sigma_0$

and we call this sequence $M_{\pm}(\tau_z)$ [32]. The first and third steps can be almost ideally implemented with composite pulses (SCROFULOUS [33]). During the second step, the ^{13}C and ^1H spins are entangled via \mathcal{H}_J and the ^1H spin decoheres simultaneously. The dynamics of the ^{13}C spin due to $M_{\pm}(\tau_z)$ is non-unitary, in contrast to the unitary control used in dynamical decoupling sequences. If we ignore the relaxation in the step (ii), $M_{\pm}(\tau_z)$ is equivalent to

$$(e^{\mp i\frac{\pi}{2}\sigma_y/2} \otimes \sigma_0) e^{-i(J\tau_z)\sigma_z \otimes \sigma_z/4} (e^{\pm i\frac{\pi}{2}\sigma_y/2} \otimes \sigma_0) = e^{\mp i(J\tau_z)\sigma_x \otimes \sigma_z/4}. \quad (18)$$

This operator entangles the spins.

We need to optimize the τ_z value in our experiments, since it should satisfy some conflicting conditions. To maximally entangle the spins, we should have $\tau_z = \frac{2\pi}{2J} \approx 2.5$ ms. To fully decohere the ^1H spin, we should have τ_z longer than T_2 for the proton spin. However, a longer τ_z reduces the QZE due to ^{13}C longitudinal relaxation.

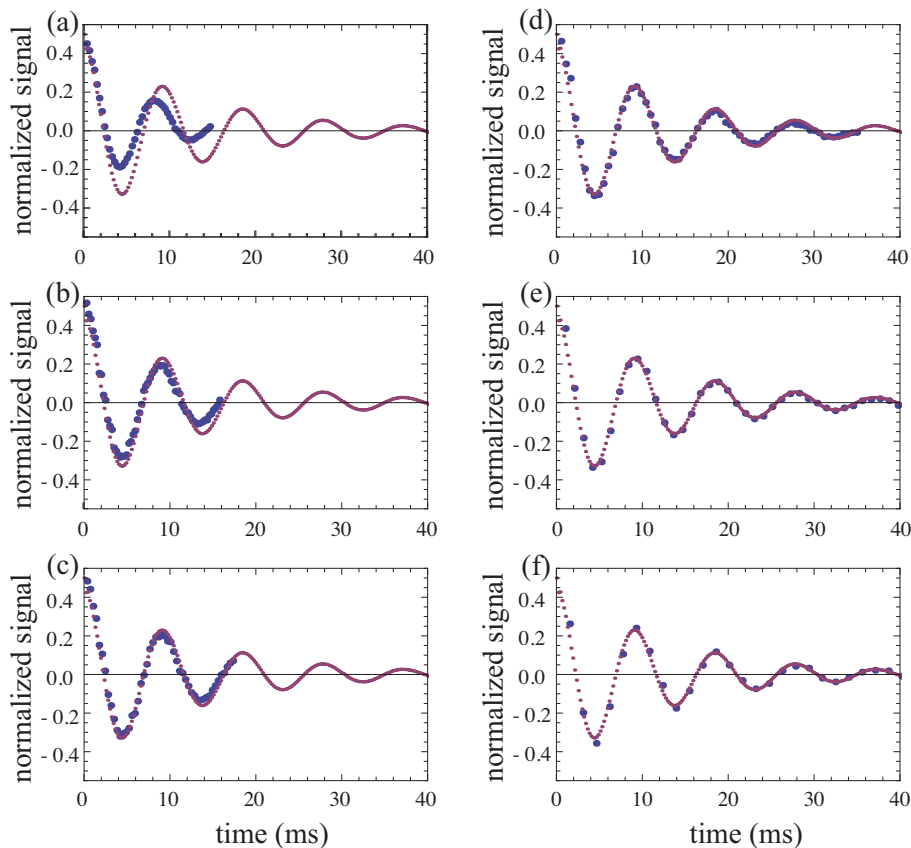
To perform the QZE experiment, we employ the pulse sequence

$$[\tau_{xy} - M_{\pm}(\tau_z)]^N, \quad (19)$$

where τ_{xy} indicates a waiting time when the phase decoherence occurs. We replace M_{DS} in Eq. (13) with a realistic $M_{\pm}(\tau_z)$, which is equally effective as a measurement.

We confirm the importance of the period τ_z in our measurement ($M_{\pm}(\tau_z)$) taking $\tau_z = 0$ in figure 6. It is easy to see that $M_{\pm}(0)$ is an identity operator from Eq. (18). Therefore, we expect that an experiment of $[\tau_{xy} - M_{\pm}(0)]^N$ reproduces the FID signal shown in figure 3, if we take into account of τ_M (the period of $M_{\pm}(0) =$ two successive composite pulses). The results with $\tau_{xy} = 0.3, 0.5, 1.0$ and 1.5 ms are identical with the FID signal. The results with $\tau_{xy} = 0.1$ and 0.2 ms are distorted, which may be caused by the fact that our spectrometer cannot produce such frequent pulses. The results described in figure 6 demonstrate that the composite $\frac{\pi}{2}$ pulses do not change the decay dynamics induced by the proton spin, as long as no entangler is applied.

Figure 6. QZE experiments with $M_-(0)$ when $\tau_{xy} =$ (a) 0.1, (b) 0.2, (c) 0.3, (d) 0.5, (e) 1.0, and (f) 1.5 ms. The x -coordinate of the n 'th point is calculated with $n(\tau_M\alpha + \tau_{xy})$, where α is a fitting parameter. $\tau_M = 2 \times 58 \mu\text{s}$ is the period of two successive composite pulses, while we choose $\alpha = 0.4$ for these experiments to reproduce the FID signal best. They are compared with the measured FID signal (small red points).



3.2.2. QZE Experiments and Simulations. The simulation of the dynamics of the ^{13}C spin during the QZE experiment is performed as follows. The pulse sequence of Eq. (19) is divided into

$$[\tau_{xy} - e^{\pm i\frac{\pi}{2}\sigma_y/2} \otimes \sigma_0 - \tau_z - e^{\mp i\frac{\pi}{2}\sigma_y/2} \otimes \sigma_0]^N,$$

where $e^{\pm i\frac{\pi}{2}\sigma_y/2} \otimes \sigma_0$ is a composite $\pi/2$ pulse acting on the ^{13}C spin in the step (i) or (iii) in $M_{\pm}(\tau_z)$. The time developments during both τ_{xy} and τ_z are calculated using the Eq. (17). Additionally, the time development ($\rho \rightarrow \rho'$) during the composite $\pi/2$ -pulse with the duration $\tau = 58 \mu\text{s}$ is calculated by

$$\rho' = (1 - (p_s + p_e)\tau) Ad(e^{-i(\mp\frac{\pi}{2}\frac{\sigma_y}{2} \otimes \sigma_0 + \mathcal{H}_J\tau)}, \rho) + p_e\tau Ad(\sigma_0 \otimes \sigma_y, \rho) + p_s\tau\rho_{th}. \quad (20)$$

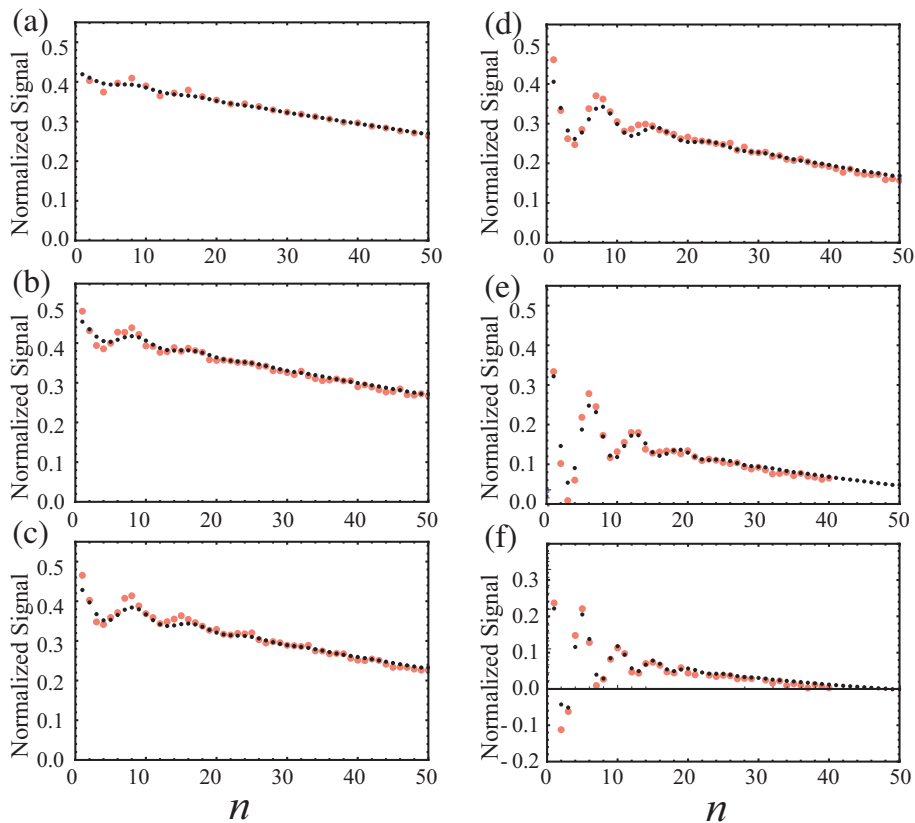
For example, in the case of $\tau_{xy} = 0.3$ ms and $\tau_z = 2.0$ ms, a detailed simulation procedure is as follows. The initial state of the experiment is $|+\rangle\langle+| \otimes \sigma_0$, which can be obtained after the application of a $\pi/2$ pulse to ρ_{th} . The output of each step is the input of the next one.

- a:** Simulating the time development during τ_{xy} with Eq. (17). We iterate this 3 times because $\tau_{xy} = 0.3$ ms and $T/N_t = 0.1$ ms.
- b:** The evolution of the state during the first rotation, $e^{\pm i\frac{\pi}{2}\sigma_y/2} \otimes \sigma_0$, is calculated using the Eq. (20).
- c:** The time development during τ_z is simulated with Eq. (17). Since $\tau_z = 2$ ms, this is iterated 20 times.
- d:** The effects of the second rotation, $e^{\mp i\frac{\pi}{2}\sigma_y/2} \otimes \sigma_0$, are taken into account using Eq. (20).

After this last step, the whole procedure is repeated N times.

Figure 7 shows the results of the QZE experiments with $M_-(\tau_z)$ varying the parameter τ_{xy} , but keeping a constant $\tau_z = 1.0$ ms. The data is compared to the simulations to check the validity of our model. We show the results with $M_-(\tau_z)$. Since the signal changes with $M_-(\tau_z)$ is larger than those with $M_+(\tau_z)$, they should be more suitable to check the quality of the simulations. Our simulations reproduce the experimental results well.

Figure 7. Measured (large red) and simulated QZE experiments (small black) with $\tau_{xy} =$ (a) 0.1, (b) 0.2, (c) 0.3, (d) 0.5, (e) 1.0, and (f) 1.5 ms in the case of $\tau_z = 1.0$ ms. The x -axis indicates n 'th measurement. We take $M_-(\tau_z)$ as a ‘‘measurement’’ in Eq. (19). $(T_d, 1/p_s) = (6.5, 300)$ ms. $T/N_t = 0.1$ ms is taken for simulations during τ_{xy} and τ_z .



The results with $\tau_{xy} \leq 0.2$ ms in figure 6 are largely distorted from the FID signal. On the other hand, a more oscillatory behaviour is observed for large τ_{xy} values, as seen in figure 7. These oscillations are originated from the J -coupling and the large oscillations indicate that the QZE is less effective. Therefore, $\tau_{xy} = 0.3$ ms is the optimal measurement frequency for the QZE demonstration with our imperfect measurement of $M_-(1.0$ ms) [31].

We vary τ_z from 0.8, 1.0, 1.2, 1.5, 2.0, and 2.5 ms in $M_{\pm}(\tau_z)$ with the constant $\tau_{xy} = 0.3$ ms, as shown in figure 8. The simulations with $M_+(\tau_z)$ are very similar to those with $T_{1s} = \infty$ (without longitudinal relaxation of the ^{13}C spin). It can be understood as follows. The state during τ_z is very close to ρ_{th} in the case of $M_+(\tau_z)$. The longitudinal relaxation given as Eq. (16) is not effective in this case since the state during τ_z are almost the same as ρ_{th} . On the contrary, the state during τ_z is very close to $|1\rangle\langle 1| \otimes \sigma_0/2$ in the case of $M_-(\tau_z)$. This process transforms the state $|1\rangle\langle 1| \otimes \sigma_0/2$ to $|0\rangle\langle 0| \otimes \sigma_0/2 = \rho_{\text{th}}$, which means the relaxation is more effective in this case. We are able to avoid most of the unwanted effects of longitudinal relaxation on the ^{13}C spin dynamics during τ_z taking $M_+(\tau_z)$ as a measurement. The longer τ_z leads to fewer oscillations of the signal, as seen in figure 8. This shows that $\tau_z \sim 2.5$ ms is long enough to implement the non-selective measurement.

The signals with $M_+(\tau_z)$ decay slower than the envelope of the FID signal, as shown in figure 8. This fact shows that the dephasing of ^{13}C spin is reduced by the QZE, since the decay of the FID signal is caused by the dephasing of the ^{13}C spin, as discussed in § 2.2. It is worth mentioning that, the only difference between the figures 6 and 8 are the existence of the entangling operations (measurements by the device), and the suppression of the decoherence in the figure 8 comes from the implementation of the measurements. Further, a single set of parameters $(T_d, 1/p_s) = (6.5, 300)$ ms for the simulations can reproduce all the experimental results well, as shown in figures 3, 7, and 8.

4. Conclusion and Discussions

We successfully suppressed the dephasing of an ensemble of spins through the application of sequential non-selective measurements. Note that these measurements does not rely on the ensemble nature of NMR. This is a proof-of-principle demonstration of the Quantum Zeno Effect suppressing non-unitary evolution.

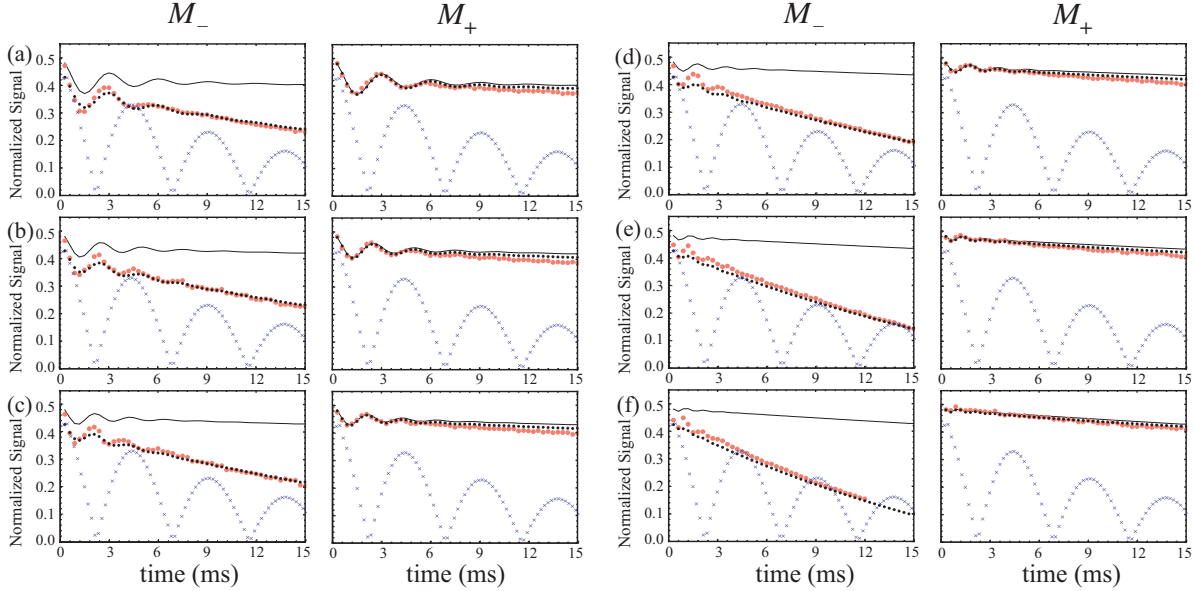
One interesting extension of this work would be the protection of an arbitrary unknown state, as discussed in the early stages of quantum information processing [34]. Here, we propose a scheme for a specific case, when $|\psi_i\rangle = \alpha|0\rangle + \beta|1\rangle$ is protected.

We encode $|\psi_i\rangle\langle\psi_i|$ to a two-qubit state by adding an ancillary qubit, as

$$\rho = |\psi\rangle\langle\psi|, \tag{21}$$

where, $|\psi\rangle = \alpha|++\rangle + \beta|--\rangle$.

Figure 8. Measured (large red) and simulated QZE experiments (small black) with $\tau_z =$ (a) 0.8, (b) 1.0, (c) 1.2, (d) 1.5, (e) 2.0, and (f) 2.5 ms in the case of $\tau_{xy} = 0.3$ ms. The x -coordinate of the n 'th point is calculated from $n\tau_{xy}$ without taking into account the measurement times $\sim n\tau_z$. $(T_d, 1/p_s) = (6.5, 300)$ ms. $T/N_t = 0.1$ ms is taken, while the pulse duration is $58 \mu\text{s}$. The solid lines are simulations when $T_{1s} = \infty$. The absolute values of the measured FID signals (\times 's) are also plotted for comparison.



The decoherence is described with the operator sum formalism as

$$\rho' = (1 - \epsilon)\rho + \frac{1}{2}\epsilon|\psi_d\rangle\langle\psi_d| + \frac{1}{2}\epsilon|\psi'_d\rangle\langle\psi'_d|, \quad (22)$$

where $|\psi_d\rangle = \alpha| - + \rangle + \beta| + - \rangle$ and $|\psi'_d\rangle = \alpha| + - \rangle + \beta| - + \rangle$.

Since the error rate ϵ is supposed to be small, we ignore the terms of order ϵ^2 or higher. We assume a quadratic decay of the first qubit, or $\epsilon = \Gamma^2 t^2$, where t is the interval between the measurements. Then, we perform the following projection operator

$$P_{\text{even}} = |++\rangle\langle++| + |--\rangle\langle--| \quad (23)$$

and we obtain

$$\rho'' = (1 - \epsilon)\rho, \quad (24)$$

although realization of P_{even} is an experimental challenge. One possible implementation of P_{even} is to use a third qubit. If we measure nonselectively this third qubit, after we entangle the third qubit with the first and second qubits, this provides us with a parity projection. When we repeat this procedure N -times in the period T , then ρ_T at the time T is

$$\rho_T = \left(1 - \Gamma^2 \left(\frac{T}{N}\right)^2\right)^N \rho. \quad (25)$$

In the limit of infinite N , we obtain $\rho_T = \rho$. ρ_T may be decoded to obtain $|\psi_i\rangle$ back.

Acknowledgments

We would like to thank Dieter Suter and Jingfu Zhang for participating in fruitful discussions and in the initial stages of this work. YK would like to thank Fumiaki Shibata, Chikako Uchiyama, and Aya Furuta for providing useful information. YK would like to thank partial supports of Grants-in-Aid for Scientific Research from JSPS (Grant No. 25400422). JGF thanks the Brazilian Funding agency CNPq (Grants No. PDE 236749/2012-9 and 300121/2015-6). YM would thank a support from JSPS KAKENHI Grant No. 15K17732.

References

- [1] Nakazato H, Namiki M and Pascazio S 1996 *Int. J. Mod. Phys. B* **10** 247
- [2] Palma G M, Suominen K A and Ekert A K 1996 *Proc. Roy. Soc. London Ser. A* **452** 567
- [3] Misra B and Sudarshan E C G 1977 *J. Math. Phys.* **18** 756
see also a recent review paper by Facchi P and Pascazio S 2008 *J. of Phys. A: Math. and Theor.* **41**, 493001 references therein
- [4] Nakazato H, Takazawa T and Yuasa K 2003 *Phys. Rev. Lett.* **90** 060401
- [5] Matsuzaki Y, Benjamin S C and Fitzsimons J 2011 *Phys. Rev. A* **84** 012103
- [6] Chin A W, Huelga S F and Plenio M B 2012 *Phys. Rev. Lett.* **109** 233601
- [7] Kwiat P, Weinfurter H, Herzog T, Zeilinger A and Kasevich M A 1995 *Phys. Rev. Lett.* **74** 4763
- [8] See, for example, Facchi P and Pascazio S 2008 *J. Phys. A: Math. Theor.* **41** 493001 references therein
- [9] Lidar D A, *Review of Decoherence-Free Subspaces, Noiseless Subsystems, and Dynamical Decoupling*, in *Quantum Information and Computation for Chemistry: Advances in Chemical Physics* Volume 154 (ed S. Kais), (John Wiley & Sons, Hoboken, New Jersey) references therein
- [10] Itano W M, Heinzen D J, Bollinger J J and Wineland D J 1990 *Phys. Rev. A* **41** 2295
- [11] Xiao L and Jones J 2006 *Physics Letters A* **359** 424
- [12] Streed E W, Mun J, Boyd J, Campbell G K, Medley P, Ketterle W and Pritchard D E 2006 *Phys. Rev. Lett.* **97** 260402
- [13] Bernu J, Deléglise S, Sayrin C, Kuhr S, Dotsenko I, Brune M, Raimond J M and Haroche S 2008 *Phys. Rev. Lett.* **101** 180402
- [14] Schafer F, et al. 2014 *Nature communications* **5** 3194
- [15] Fischer M C, Gutiérrez-Medina B and Raizen M G 2001 *Phys. Rev. Lett.* **87** 040402
- [16] Álvarez G A, Rao D D B, Frydman L and Kurizki G 2010 *Phys. Rev. Lett.* **105** 160401
- [17] Matsuzaki Y, Saito S, Kakuyanagi K and Semba K 2010 *Phys. Rev. B* **82** 180518
Matsuzaki Y and Tanaka H 2012 arXiv:1209.3136
Matsuzaki Y and Tanaka H 2016 *J. Phys. Soc. Jpn.* **85** 014001
- [18] Balzer C, Hannemann Th, Reiß D, Wunderlich Chr, Neuhauser W, and Toschek P E 2002 *Opt. Commun.* **211** 235, Toschek P E and Wunderlich Ch 2001 *Eur. Phys. J. D* **14** 387
- [19] See, for example, Kondo Y et al. 2007 *J. Phys. Soc. Jpn.* **76** 074002 references therein
- [20] Gardiner C W and Zoller P, *Quantum noise: a handbook of Markovian and non-Markovian quantum stochastic methods with applications to quantum optics*, Vol. **56**, (Springer, 2004)
- [21] See, for example, Abragam A, *Principles of Nuclear Magnetism*, (Oxford University Press, New York, 1989)
- [22] Levitt M H, *Spin Dynamics*, (John Wiley and Sons, New York, 2008)
- [23] Zurek W H 2003 *Rev. Mod. Phys.* **75** 715
- [24] Nielsen M A and Chuang I L, *Quantum Computation and Quantum Information* (Cambridge University Press, 2000)

- [25] See, for example, De Lange G, et al. 2010 *Science* **330** Issue 6000 60 references therein
- [26] Barnum H, Nielsen M A and Schumacher B 1998 *Phys. Rev. A* **57** 4153
- [27] Nakahara M, Kondo Y, Hata K and Tanimura S 2004 *Phys. Rev. A* **70** 052319
- [28] Ali Ahmed M A, Álvarez G A and Suter D 2013 *Phys. Rev. A* **87** 042309 references therein
- [29] Gullion T, Baker D B and Conradi M S 1990 *J. Magn. Reson.* **89** 479
- [30] Yuge T, Sasaki S and Hirayama Y 2011 *Phys. Rev. Lett.* **107** 170504
Álvarez G A and D. Suter 2011 *Phys. Rev. Lett.* **107** 230501
- [31] Facchi F, Nakaguro Y, Nakazato H, Pascazio S, Unoki M, and Yuasa K 2003 *Phys. Rev. A* **68**
012107
- [32] Kondo Y 2007 *J. Phys. Soc. Jpn.* **76** 104004
- [33] Cummins H K, Llewellyn G, and Jones J A 2003 *Phys. Rev. A* **67** 042308
- [34] Barenco A, Berthiaume A, Deutsch D, Ekert A, Jozsa R and Macchiavello C 1997 *S. I. A. M. Journal on Computing* **26-5** 1541